Available online at www.sciencedirect.com
SCIENCE DIRECT
Chemical Physics 324 (2006) 507–514
Chemical Physics
www.elsevier.com/locate/chemphys

Classical and quantum dynamics of the O + CN reaction

Erik Abrahamsson [a,*], Stefan Andersson [a], Gunnar Nyman [a], Nikola Marković [b]

[a] Department of Chemistry, Physical Chemistry, Göteborg University, SE-412 96 Göteborg, Sweden
[b] Physical Chemistry, Department of Chemical and Biological Engineering, Chalmers University of Technology, SE-412 96 Göteborg, Sweden

Received 8 July 2005; accepted 9 November 2005
Available online 27 December 2005

Abstract

Electronic structure (CASPT2) calculations have been performed for the lowest $^2\Pi$ and $^4\Sigma^-$ states of the NCO system. To create the potential energy surfaces, the generalized discrete variable representation (GDVR) method has been used. Wave packet calculations have been performed for the collinear O + CN reaction on both surfaces. These are the first reported quantum dynamics calculations on this reaction. State-to-state reaction probabilities are presented. On the $^2\Pi$ surface, which has an almost 6 eV deep well, we obtain structure in the reaction probabilities at low kinetic energies but at higher energies they are smooth. The $^4\Sigma^-$ surface is highly exoergic and vibrationally non-adiabatic dynamics is observed. The $^4\Sigma^-$ surface has an early barrier and as a result we find that translational energy more efficiently promotes the reaction than vibrational energy does. The wave packet results are compared with QCT results. Generally the agreement is good as would be expected but some notable differences are found, particularly for reaction out of the vibrational ground state.

Keywords: Quantum dynamics; Classical dynamics; Wavepacket; Quasiclassical trajectory; Reactive scattering; NCO; O + CN; Interpolated potential energy surface

1. Introduction

The reactive system O + CN has received attention as a possible major source of depletion of CN in both combustion [1] and in dense interstellar clouds [2,3]. This study is concerned with the dynamics of the reaction of ground state oxygen atoms with cyanogen radicals,

$$O(^3P) + CN(X^{2+}) \rightarrow CO(X^{1+}) + N(^2D), \quad (1)$$

and

$$O(^3P) + CN(X^{2+}) \rightarrow CO(X^{1+}) + N(^4S). \quad (2)$$

It is believed that reaction (1) is the most important source of CN destruction in interstellar clouds. The detailed knowledge of the O + CN reaction could be crucial for the understanding of the chemical evolution in interstellar clouds, as CN is a possible precursor to complex molecules, such as cyanopolyynes.

Detailed studies of reactions (1) and (2) were performed in the 1970s by Schmatjko and Wolfrum, involving both quasiclassical trajectory (QCT) calculations on empirical LEPS type potential energy surfaces and experimental investigations of the dynamics and kinetics [4,5]. From their room temperature experiments they inferred that about 20% of the reactive events produced $CO(X^1\Sigma^+) + N(^4S)$, corresponding to reaction (2) above.

Statistical adiabatic channel model (SACM) calculations have been published on the rate coefficients of reaction (1) at $T = 300$–5000 K [6]. We have also performed QCT calculations for the rate coefficient on the same reaction for T between 5 and 5000 K using ab initio based potential energy surfaces [7]. Apart from the mentioned QCT and SACM calculations, no computational studies have been published on the dynamics of these reactions.

Quantum dynamical calculations are demanding for the NCO system due to the deep potential wells and the

* Corresponding author. Tel.: +46 31 772 30 61; fax: +46 31 772 13 94.
E-mail addresses: abrahams@chem.gu.se (E. Abrahamsson), nyman@chem.gu.se (G. Nyman).

0301-0104/$ - see front matter © 2005 Elsevier B.V. All rights reserved.
doi:10.1016/j.chemphys.2005.11.012

occurrence of three heavy atoms. Previously, Monnerville et al. have performed 2D [8] and 3D [9] wave packet dynamics calculations on the C + NO reaction, using a PES containing the linear CNO minimum but not the deeper NCO minimum, which made the 3D study possible for a total angular momentum of zero. Recently Abrol and collaborators [10] performed 2D wave packet calculations for the collinear C + NO → CN + O reaction, observing resonances.

Extensive computational studies of the structure and properties of the NCO complex have been performed in the last few years [11,12]. The molecule has also been the subject of several experimental studies (see Ref. [12]). A complete wave packet study for the NCO system on a potential energy surface including the deeper NCO minimum is still not feasible. In this study, we therefore report collinear 2D calculations for the two reactions listed above. Using the collinear approach on the $^2\Pi$ surface is motivated since the NCO complex is linear, and the long-range attraction between O and CN is strongest in the collinear configuration [7]. For the $^4\Sigma^-$ surface a collinear study may be a less realistic model.

In this paper, we first report collinear potential energy surfaces for reactions (1) and (2) based on ab initio calculations and an interpolation method developed previously [13]. Thereafter wave packet calculations are reported for both reactions. It is expected that for reactions involving three relatively heavy elements, as in the present case, quantum effects should be small or negligible. We investigate this by performing QCT calculations and comparing the results with the wave packet calculations. Largely the quantum and QCT results agree but differences are also observed and discussed.

2. Computational aspects

2.1. Potential energy surface

Electronic structure calculations were performed using the MOLCAS 5.2 program package [14]. We employed the CASPT2 method with the g_1 Fock matrix and an ANO-L basis set with the 14s9p4d3f primitive set contracted to 4s3p2d1f. Calculations were made for the lowest $^2\Pi$ and $^4\Sigma^-$ electronic states for collinear geometries of the NCO system and also for the CN($X^2\Sigma^+$) and CO($X^1\Sigma^+$) molecules.

The generalized discrete variable representation (GDVR) method [13,15] was used to interpolate a smooth energy surface using 484 energy points for each surface. There were 22 points for each coordinate (R_{CN} and R_{CO}) in a range from 0.83 to 12.97 Å. The points were evenly distributed in the coordinate $x_i = \ln R_i$ ($R_i = R_{CN}$ or R_{CO}). This means that the grid in the R_i coordinate was denser the smaller the values of R_i, giving a detailed description of the reaction zone. For each surface 171 points were calculated by CASPT2.

In the long-range region 144 points were calculated using a dispersion type $-C_6/R^6$ energy expression, where R is the usual Jacobi coordinate. In the O + CN channel a C_6 parameter was determined for each R_{CN}-value using the two CASPT2 points with the largest R_{CO}-values. A similar procedure was used in the N + CO channel. For stretched geometries (R_{CN} and R_{CO} both larger than 2.4 Å) 169 points were calculated as the sum of diatomic potentials (CN and CO). The diatomic potential curves were interpolated in an analogous manner as for NCO with 18 points for CN distributed between 0.80 and 13.59 Å and 30 points for CO between 0.80 and 13.12 Å.

2.2. Quantum scattering calculations

The time-dependent wave packet calculations were carried out in mass-weighted product Jacobi coordinates $(\tilde{R}, \tilde{r})$, using the Hamiltonian

$$\hat{H} = -\frac{\hbar^2}{2\mu}\left(\frac{\partial^2}{\partial\tilde{R}^2} + \frac{\partial^2}{\partial\tilde{r}^2}\right) + V(\tilde{R}, \tilde{r}), \tag{3}$$

where $\tilde{R}$ is the mass-weighted center-of-mass separation between N and CO, $\tilde{r}$ is the mass-weighted CO bond distance, and the reduced mass μ is given by

$$\mu = \left(\frac{m_O m_C m_N}{m_O + m_C + m_N}\right)^{1/2}. \tag{4}$$

The product Jacobi coordinates are given by

$$R = \alpha^{-1}\tilde{R}, \tag{5}$$

$$r = \alpha\tilde{r}, \tag{6}$$

where $\alpha = (\mu_R/\mu_r)^{1/4}$ and μ_R and μ_r are the reduced masses corresponding to the N–CO and CO systems, respectively. The initial wave packet is set up in reactant Jacobi coordinates, as a product of a vibrational eigenfunction of the CN system, $\phi(r_{CN})$, and a translational function in the form of a Gaussian wave packet, $\chi(R_{O\text{–}CN})$,

$$\Psi(R_{O\text{–}CN}, r_{CN}, t = 0) = \phi_v(r_{CN})\chi(R_{O\text{–}CN}). \tag{7}$$

The wave function is then transformed to product Jacobi coordinates before the propagation begins. The vibrational eigenfunctions needed for the initialization and analysis are obtained by solving the time-independent Schrödinger equation for the diatomic fragments using a sine-basis expansion of the wave function.

The wave packet is propagated by solving the time-dependent Schrödinger equation using the split-operator method [16]. Reflection of the wave packet from the grid boundary is avoided by applying a damping function between $r_i = r_d$ and r_{max} ($r_i = \tilde{R}$ or $\tilde{r}$):

$$f(r_i) = \begin{cases} 1, & r_i < r_d, \\ \exp[-V_d\Delta t/\hbar], & r_i \geqslant r_d, \end{cases} \tag{8}$$

where V_d is the exponential damping function suggested by Vibók and Balint-Kurti [17]. By introducing a time-dependent scale factor in the exponential damping function V_d, the lowering of the average product kinetic energy with propagation time was taken into account.

Before damping, the scattered wave packet is projected onto asymptotic vibrational eigenstates at $R = R_p$

$$c_{v'}(t) = \int \mathrm{d}r \phi_{v'}(r) \Psi(R_p, r, t). \quad (9)$$

The time-dependent amplitudes $c_{v'}$ are Fourier transformed to energy space

$$b_{v'} = \frac{1}{\sqrt{2\pi}} \int \mathrm{d}t c_{v'}(t) \exp(\mathrm{i}Et/\hbar), \quad (10)$$

and the state-to-state reaction probabilities are computed from the ratio between the scattered and incident fluxes [18],

$$P_{v \to v'}(E) = \frac{F_{v'}(E)}{F_v(E)}, \quad (11)$$

where

$$F_{v'}(E) = \frac{1}{\mu_{OC-N}} k_{v'} |b_{v'}(E)|^2, \quad (12)$$

$$k_{v'} = \frac{1}{\hbar} \sqrt{2\mu_{OC-N}(E - V(R_p) - E_{v'})}. \quad (13)$$

The incident flux is, in principle, given by an analytical expression [18], but since the potential has not reached its true asymptotic value at the position of the initial wave packet, a small correction is needed. The correction is simply to obtain the probability distribution of the incident k-values by propagating the initial Gaussian wave packet $\chi(R)$ backwards, and to use this k-distribution to normalize the scattered components rather than to use the initial Gaussian distribution.

2.3. Numerical details

The wave packet propagations were carried out for both r and R in the range from 0.5 to 12.5 Å on a grid with 1680 points in each coordinate. The time step was 0.1 fs, and the propagations were continued until more than 99.5% of the wave packet had left the grid. The damping was applied from $r_d = 9.51$ Å to R_{max} in both channels. The analysis of the outgoing wave packet was done at $R_p = 9.5$ Å. The initial wave packet was centered at an R_{CO} distance of 8.5 or 9.5 Å.

Several grid sizes, from 1008 to 5040 points in each coordinate, and different time steps, from 0.05 to 0.3 fs, were used to test the convergence of the parameters. The outgoing wave packet was analyzed in an energy interval corresponding to 95% of the energy distribution in the incident Gaussian.

The collinear QCT calculations were carried out in Cartesian coordinates using the same trajectory program as previously used in the 3D case [7]. The initial O–CN separation was 14 Å (the potential energy surface is defined but flat outside the interpolation region) and the CN bond length and vibrational phase were sampled micro-canonically at the considered initial vibrational energy. The gradient of the interpolated potential was obtained numerically using a finite difference approximation. Good energy conservation was observed.

To obtain the product vibrational quantum number in the QCT calculations, the energy difference $|E'_{vib} - E_{v'}|$, where E'_{vib} is the final vibrational energy and $E_{v'}$ are the CO eigenvalues, was minimized. The product CO molecule is then assigned the vibrational quantum number corresponding to $E_{v'}$. The trajectory results for the $^2\Pi$ surface are converged to within the size of the symbols in Figs. 3 and 4. For the $^4\Sigma^-$ surface 10,000 trajectories were used to obtain the total reaction probabilities for each set of initial conditions. The product vibrational distributions on the quartet surface are based on approximately 10,000 *reactive* trajectories.

3. Results and discussion

3.1. Potential energy surface

In Fig. 1 contour plots of the two interpolated potential energy surfaces are shown. It is seen that both surfaces are smooth and well-behaved. The 'potential groove' which is seen on the $^2\Pi$ surface for $R_{CO} \approx 2.7$ Å and $R_{CN} > 2.5$ Å is due to the fact that the surface correlates with N(^{2}D) in the N + CO channel but with N(^{4}S) in the atomization limit. The 'groove' is caused by an avoided crossing with a $^2\Pi$ surface correlating with N(^{4}S) and an *excited* electronic state of CO. This part of the potential is however not accessed by the dynamics considered in this work, and should have no impact on the final results.

We have calculated minimum energy paths on both the $^2\Pi$ and $^4\Sigma^-$ surfaces. These are shown in Fig. 2. Stationary points along the reaction coordinate are summarized in Table 1. There are noticeable differences between the calculated and the experimental data for the NCO molecule. However, the values presented here are close to the values calculated in recent high-level ab initio studies [11,12].

It is seen that there are drastic differences in the shapes of the surfaces. Both surfaces are exothermic, with an energy difference of 0.81 eV for the $^2\Pi$ surface and 3.39 eV for the $^4\Sigma^-$ surface. While the $^2\Pi$ surface is quite attractive in the O + CN channel, and has a 5.85 eV deep potential well, the $^4\Sigma^-$ surface is only weakly attractive in the O + CN long-range region, and it exhibits a potential barrier of 1.42 eV, which results in a barrier height of 1.37 eV when the harmonic zero-point energy is taken into consideration. It is thus only on the $^2\Pi$ surface that reaction is thermally accessible at room temperature.

3.2. Scattering calculations on the $^2\Pi$ surface

Fig. 3 shows the total and state-to-state reaction probabilities for the case where the initial wave packet has a mean translational energy, $\overline{E}_{kin}$, of 1.00 eV with CN in the vibrational ground state ($v = 0$). The total propagation time is 2 ps. In the energy interval considered, nine different

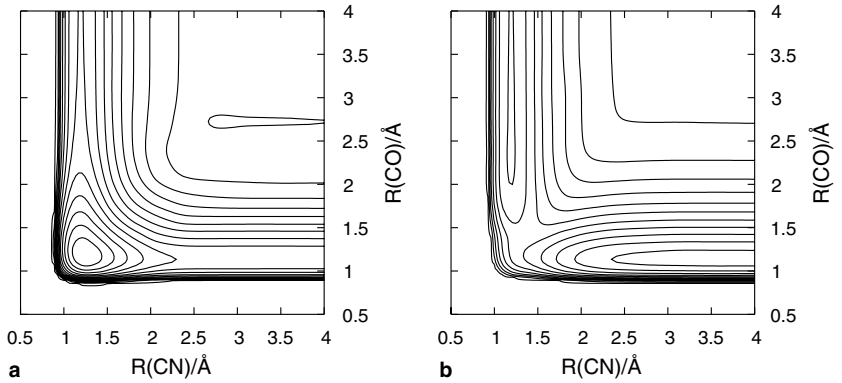

Fig. 1. Contour plots of the N–C–O electronic potential energy surfaces for the: (a) $^2\Pi$ and (b) $^4\Sigma^-$ configurations. The spacing between the contours is 1.0 eV.

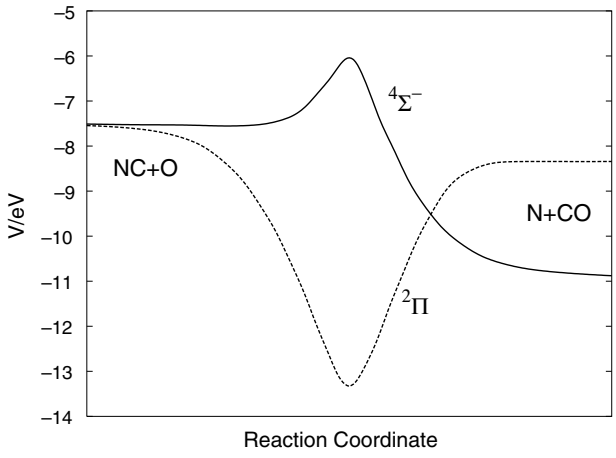

Fig. 2. Minimum energy paths connecting O + CN and N + CO for the $^2\Pi$ and $^4\Sigma^-$ potential energy surfaces. The energies are relative to separated atoms.

Table 1
Characteristics of the $^2\Pi$ and $^4\Sigma^-$ interpolated PESs

	R_{CN} (Å)	R_{CO} (Å)	V (eV)	ω_1 (cm^{-1})	ω_2 (cm^{-1})
The $^2\Pi$ surface					
O + CN	1.194	–	−7.479	1850	–
N + CO	–	1.132	−8.293	2115	–
N–CO	3.117	1.132	−8.344	2129	54
N–CO TS	2.801	1.131	−8.341	2134	71i
NCO	1.239	1.196	−13.333	2014	1217
	1.200	*1.206*	–	*1921*	*1267*
The $^4\Sigma^-$ surface					
O + CN	1.195	–	−7.459	1846	–
N + CO	–	1.133	−10.852	2115	–
NCO TS	1.287	1.393	−6.041	1028	1449i

Energies are relative to separated atoms.
Calculated frequencies are harmonic. Experimental data (in italic) are taken from Ref. [19] and Ref. [11]. The experimental frequencies are fundamentals.

vibrational states are allowed in the product channel, but only $v' = \{0,4\}$ contribute notably to the reaction probability.

It is seen in Fig. 3 that the total reaction probability is constant at 1.0. Thus, all incoming reactants form products, throughout the energy interval. The state-to-state reaction probabilities depend weakly on the total energy and there is a slight shift from formation of ground state CO ($v' = 0$) to vibrationally excited CO in the $v' = 1$ state, as the total energy is increased. Propagation of a wave packet with an initial average kinetic energy of 0.5 eV gives similar results.

The QCT results in Fig. 3 show obvious similarities with the wave packet results but also surprising differences. Only $v' = \{0,2\}$ contribute to the reaction probability and it is notable that the $v' = 2$ population is slightly larger than the $v' = 1$ population, contrary to the wave packet results.

The differences between the quantum and classical results in Fig. 3 may be specific to the initial condition $v = 0$. In this quantum state the classical and quantum probability distributions differ maximally and we generally expect largest differences between classical and quantum results for small vibrational quantum numbers. We will return to this issue in presenting the results for the $^4\Sigma^-$ surface.

The total and state-to-state reaction probabilities for a wave packet initially in the ground state and with a mean translational energy of 0.06 eV are presented in Fig. 4. The total propagation time is 20 ps. The total reaction probability is still 1.0, but the state-to-state reaction probabilities show a mildly resonant behavior. Notable are the relatively large changes in the $v = 0 \rightarrow v' = 0$ and $v = 0 \rightarrow v' = 1$ transition probabilities at some energies, particularly around 0.15, 0.17 and 0.225 eV. These are quantum effects, which thus appear for this system with three rather heavy atoms, treated collinearly.

Quantum effects were observed also by Abrol et al. [10], who performed collinear time-independent quantum dynamics calculations on the C + NO reaction at low energies. It remains an open question as to whether quantum effects are also clearly visible in a three-dimensional treatment of the dynamics. Preliminary results by Monnerville et al. [9] on the C + NO reaction indicate that this might be the case.

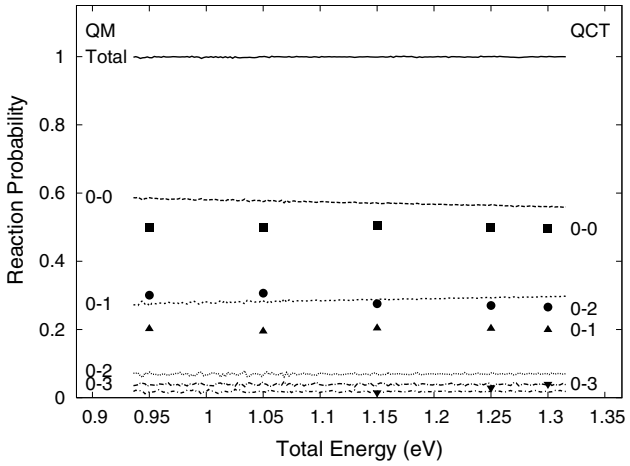

Fig. 3. Total and state-to-state reaction probabilities for a wave packet initially in $v = 0$ with $\overline{E}_{kin}$=1.0 eV on the $^2\Pi$ surface. Lines represent quantum results. The values of $v - v'$ are noted to the left of each line. Symbols represent quasiclassical results. The values of $v - v'$ are noted to the right.

The QCT results shown in Fig. 4 are similar to the ones in Fig. 3. It is noticed that the fluctuations seen in the wave packet results are not present in the QCT results. We also note that the reaction is fast on the $^2\Pi$ surface even though there is a 5.85 eV deep well. This holds both for the quantum and classical results. Classically a complex with a lifetime between 10 and 12 fs is formed, which in this case corresponds to three minimum distance exchanges. The complex is defined to live from the first internuclear minimum distance exchange until the last [20]. Quantum mechanically the complex is considered to exist in the region illustrated in Fig. 5. By calculating the flux in and out of this area as a function of time a lifetime of the complex can be estimated to be approximately 20 fs. It is also seen in Fig. 5 that a small part of the wave packet remains in the potential well for a long time.

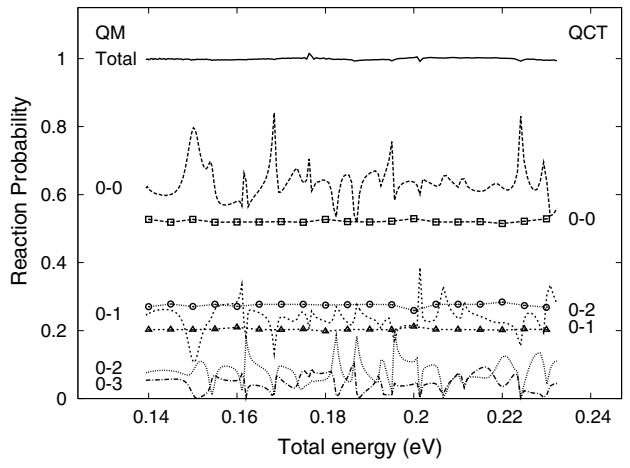

Fig. 4. Total and state-to-state reaction probabilities for a wave packet initially in $v = 0$ and with $\overline{E}_{kin} = 0.06$ eV on the $^2\Pi$ surface. Lines represent quantum results. The values of $v - v'$ are noted to the left of each line. Symbols represent quasiclassical results. The values of $v - v'$ are noted to the right.

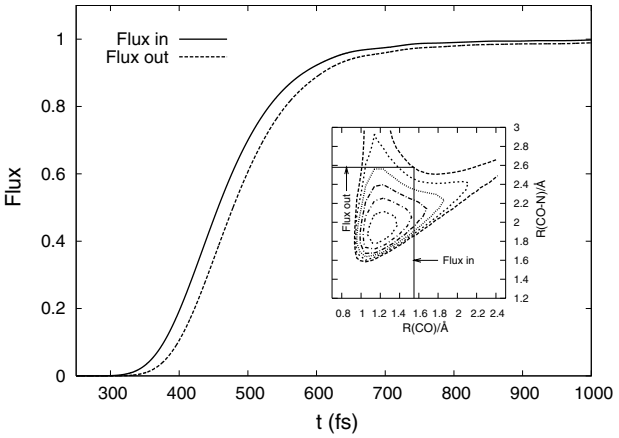

Fig. 5. The flux in and out of the potential well as a function of time. The inset shows the regime in which a complex is considered to exist.

Classically the complete reaction, considered as beginning and ending when the center-of-mass separation between the fragments are 10 Å, takes about 1 ps. The wave packets results are similar except that a small percentage (1–2%) of the wavepacket, particularly the low energy components, remains in the well for a long time, necessitating a long propagation time.

To confirm the results of the wave packet calculations, several grids, time steps, damping parameters, and propagation times were used with a wave packet initially in $v = 0$ and with $\overline{E}_{kin} = 0.06$ eV. In Fig. 6 the total reaction probability, as well as the $v = 0 \rightarrow v' = 0$ and $v = 0 \rightarrow v' = 1$ state-to-state reaction probabilities, for several different calculations are shown. It can be seen that the difference between the cases is minimal, and we can conclude that a grid with 1680×1680 grid points is sufficient.

3.3. Scattering calculations on the $^4\Sigma^-$ surface

In Fig. 7, state-to-state reaction probabilities are shown for reaction out of the ground vibrational state for total energies of 1.45, 1.60 and 1.80 eV. The reaction probabili-

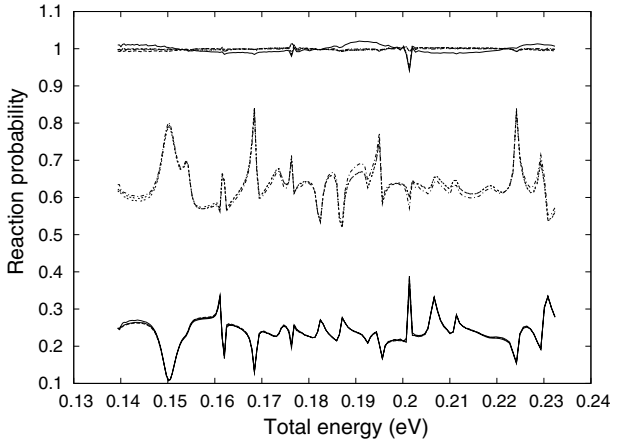

Fig. 6. Total, $v = 0 \rightarrow v' = 0$, and $v = 0 \rightarrow v' = 1$ state-to-state reaction probabilities for a wave packet with $\overline{E}_{kin} = 0.06$ eV on the $^2\Pi$ surface. Grid sizes: 1008, 1680, 2520, and 5040 points in each coordinate. Propagation times: 10 and 20 ps.

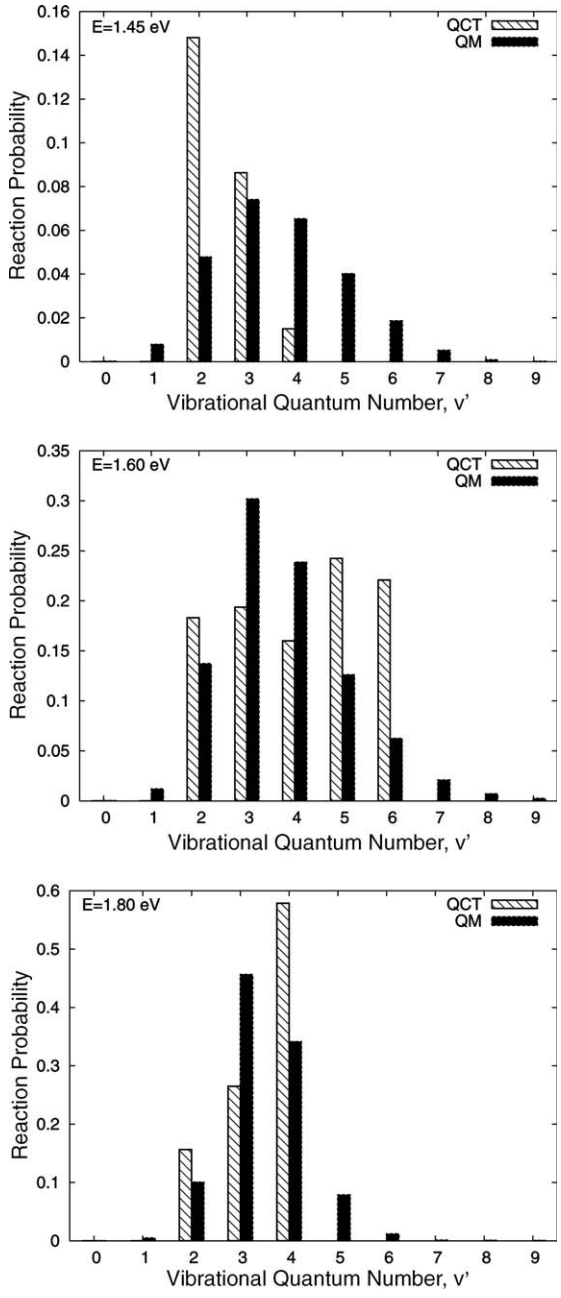

Fig. 7. State-to-state reaction probabilities at different total energies (1.45, 1.60 and 1.80 eV) for wave packets initially in $v = 0$ on the $^4\Sigma^-$ surface. Note the different scales on the reaction probability axes in the various panels.

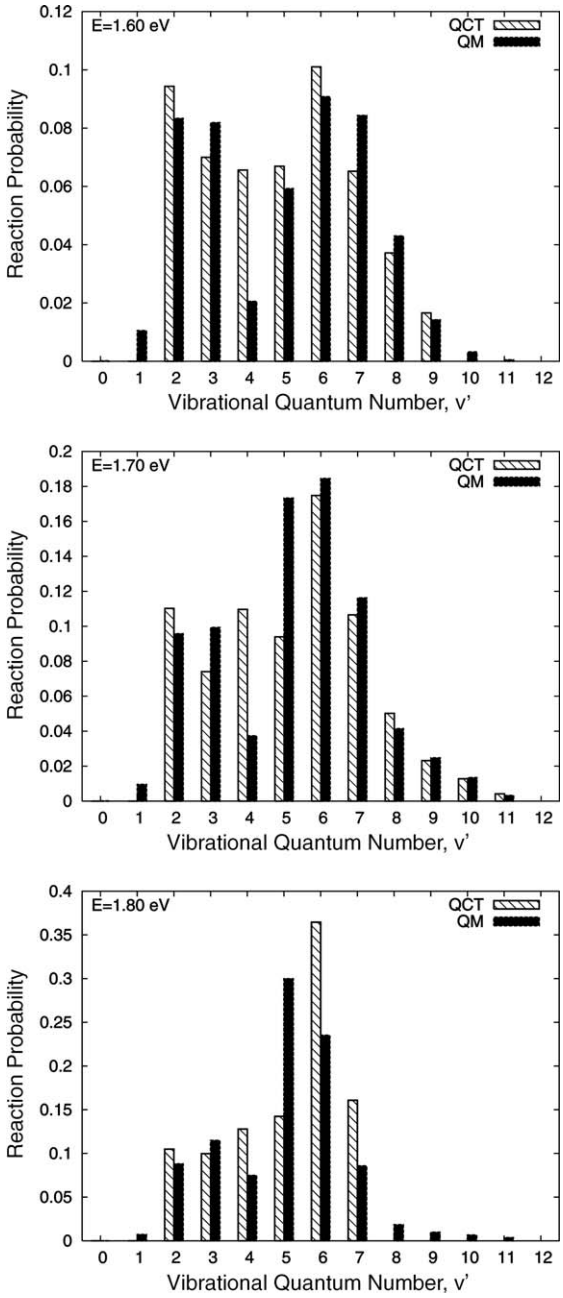

Fig. 8. State-to-state reaction probabilities at different total energies (1.60, 1.70, and 1.80 eV) for wave packets initially in $v = 1$ on the $^4\Sigma^-$ surface. Note the different scales on the reaction probability axes in the various panels.

ties increase as the vibrational product excitation increases from $v' = 0$ to $v' = 3$, and decrease from $v' = 4$ and upwards. $v' = 22$ is the highest state allowed for a wave packet with a total energy of 1.80 eV but it is seen that there is no significant population beyond $v' = 9$. The QCT results in Fig. 7 are quite different from the wave packet results. They have different overall shapes and generally populate a smaller number of product vibrational states.

In Fig. 8, state-to-state reaction probabilities are shown for reaction out of the first excited vibrational state for total energies of 1.60, 1.70 and 1.80 eV. The state-to-state reaction probabilities now show a less systematic pattern. The transition from $v = 1$ to $v' = 0$ is too weak to be seen in this figure. The QCT results are here in better agreement with the wave packet calculations than what was the case in Fig. 7. This is again true when studying the wave packet and QCT results for reaction out of the second excited state, Fig. 9.

The results in Figs. 7–9 agree with the notion that quantum and classical results agree better the higher the vibrational quantum number is. For the CNO system with

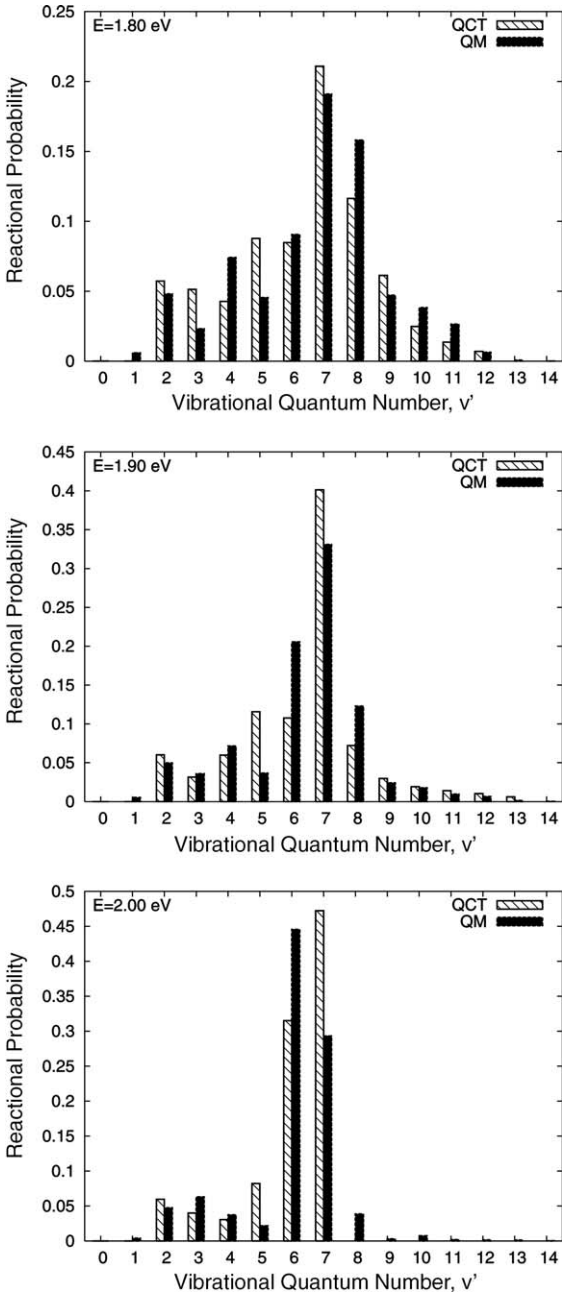

Fig. 9. State-to-state reaction probabilities at different total energies (1.80, 1.90, and 2.00 eV) for wave packets initially in $v = 2$ on the $^4\Sigma^-$ surface. Note the different scales on the reaction probability axes in the various panels.

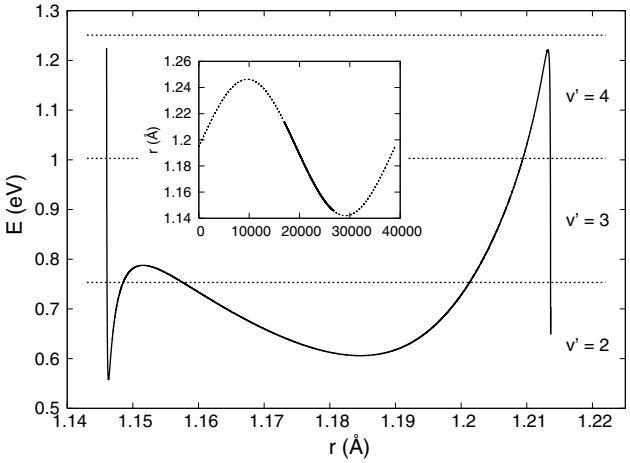

Fig. 10. Product vibrational energy as function of initial C–N distance on the $^4\Sigma^-$ surface, $v = 0$, E_{tot}=1.45 eV. The dotted horizontal lines show the energies used to assign vibrational quantum numbers to the CO product. The inset shows initial C–N distance versus trajectory number. The solid line represents reactive trajectories, the dotted line non-reactive.

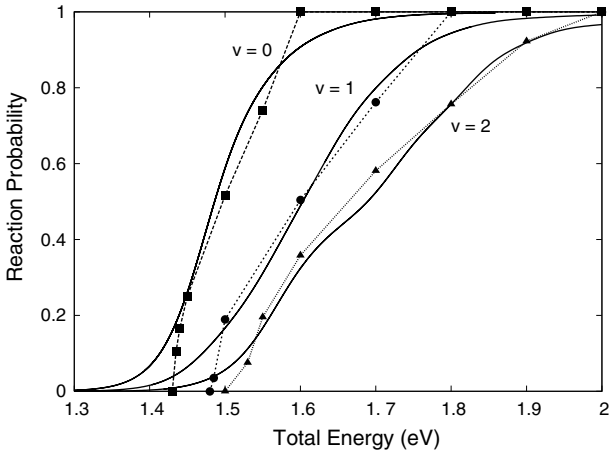

Fig. 11. Total reaction probabilities as a function of total energy for wave packets initially in different vibrational states on the $^4\Sigma^-$ surface. Solid lines represent quantum results, lines with symbols represent quasiclassical results.

three relatively heavy atoms the quantum effects seem to be significant primarily for $v = 0$. We observe that the classical product vibrational distributions are always narrower than their corresponding quantum distributions. This is to be expected as the phase space distribution resulting from a Wigner transform of the quantum distribution will include a spread of energies (in this way also accounting for tunneling), thereby widening and smoothing the classical distribution.

There is a direct relation between the classically determined product vibrational energy and the initial vibrational phase of the trajectory, as shown in Fig. 10. Analyzing this relation makes it clear that the differences between the classical and quantum distributions originate in the different initial probability distributions. With this in mind the results in Figs. 7–9 seem to be rationalized.

The total reaction probabilities for the cases where the initial wave packets and quasiclassical trajectories are in the vibrational states $v = 0$, $v = 1$, and $v = 2$, respectively, are presented in Fig. 11. It can be seen that slight tunneling occurs, as the reaction probability is non-zero for energies below the vibrationally adiabatic ground state (VAG) barrier height, 1.37 eV. The tunneling probability is about 2.5% at the barrier height.

In Fig. 11 it is seen that higher vibrational excitation in the reactant leads to lower reaction probabilities, for a given total energy. Thus, kinetic energy promotes reaction more efficiently than vibrational energy. This can be

explained by the fact that the barrier is early in the reaction path, and the reactants need to have sufficient kinetic energy to pass the barrier.

The QCT results in Fig. 11 generally agree well with the wave packet results but differences are seen at small and large (close to unity) reaction probabilities (less for $v = 2$ than for $v = 0$ and $v = 1$). Note that the classical barrier height is 1.42 eV which enhances the effective difference between the QCT results and the wave packet results as the VAG barrier height is 0.05 eV lower.

4. Summary

We have constructed 2D potential energy surfaces for the $^2\Pi$ and $^4\Sigma^-$ electronic states of the $O + CN \rightarrow CO + N$ reaction in collinear geometries. Ab initio data obtained from CASPT2 electronic structure calculations and other information have been used to generate 484 energy data points for each surface. These data points are interpolated by a generalized DVR procedure previously developed by Yu, Andersson and Nyman [13].

Time-dependent wave packet calculations using the split-operator propagator have been performed on both surfaces in product Jacobi coordinates. The results on the $^2\Pi$ surface, which is barrierless with a deep well, show structure in the reaction probabilities as a function of energy up to about 0.5 eV translational energy.

On the $^4\Sigma^-$ surface, which has a 1.42 eV high classical barrier and large exothermicity, the reaction is highly vibrationally non-adiabatic with initial translational energy more efficient in promoting the reaction than initial vibrational excitation. This is not surprising as the reaction has an early transition state. We also noted a difference in the lowest energy for which reaction occurs classically and quantum mechanically on the $^4\Sigma^-$ surface. This is largely due to the fact that the classical barrier height (1.42 eV) and the vibrationally adiabatic ground state barrier height (1.37 eV) differ by 0.05 eV, but partly also due to tunneling.

For reaction out of $v = 0$ on the $^4\Sigma^-$ surface, the wave packet results show a systematic trend of increasing reaction probabilities for increasing product vibrational excitation up to $v' = 3$, thereafter the reaction probabilities decrease with further increasing product vibrational excitation. For reaction out of $v = 1$ and $v = 2$ these systematic trends are not observed.

In comparing the wave packet results with the QCT results we observed that differences in the product vibrational distributions primarily appear from reaction out of $v = 0$, which is related to the significant difference in initial classical and quantum distributions for $v = 0$. Also on the $^2\Pi$ surface differences between the product distributions where observed for reaction out of $v = 0$.

It would be interesting to be able to perform comparisons between quantum and classical dynamics calculations in full-dimensionality for this reaction involving three relatively heavy atoms and deep wells. It is quite feasible that the differences would then be washed out when producing cross sections by averaging the results over many values of the total angular momentum (or the impact parameter). However, Abrol et al. [10] performed 2D wave packet calculations on the C + NO reaction and suggested that the resonances they observed may survive in 3D calculations. They in fact speculated that the resonances would survive in the 'real world' and it would be fascinating if this could be investigated.

Acknowledgement

Support from the Swedish Science Research Council is gratefully acknowledged.

References

[1] C. Schulz, H.-R. Volpp, J. Wolfrum, Chemical Dynamics in Extreme Environments, World Scientiffic, Singapore, 2001, p. 206.
[2] E. Herbst, W. Klemperer, Astrophys. J. 185 (1973) 505.
[3] E. Herbst, H.-H. Lee, D. Howe, T. Millar, Mon. Not. R. Astron. Soc. 268 (1994) 335.
[4] K.J. Schmatjko, J. Wolfrum, J. Ber. Bunsenges. Phys. Chem. 79 (1975) 696.
[5] K.J. Schmatjko, J. Wolfrum, J. Ber. Bunsenges. Phys. Chem. 82 (1978) 419.
[6] C.J. Cobos, React. Kinet. Catal. Lett. 57 (1996) 43.
[7] S. Andersson, N. Marković, G. Nyman, J. Phys. Chem. 107 (2003) 5439.
[8] M. Monnerville, P. Halvick, J. Rayez, J. Chem. Soc., Faraday Trans. 89 (1993) 1579.
[9] M. Monnerville, G. Peoux, S. Briquez, P. Halvick, Chem. Phys. Lett. 322 (2000) 157.
[10] A. Abrol, L. Wiesenfeld, B. Lambert, A. Kuppermann, J. Chem. Phys. 114 (2001) 7461.
[11] R. Prasad, J. Chem. Phys. 120 (2004) 10089.
[12] M.S. Schuurman, S.R. Muir, W.D. Allen, H.F. Schaefer III, J. Chem. Phys. 120 (2004) 11586.
[13] H.G. Yu, S. Andersson, G. Nyman, Chem. Phys. Lett. 321 (2000) 275.
[14] K. Andersson, A. Barysz, A. Bernhardsson, M.R.A. Blomberg, D. Carissan, L. Cooper, M. Cossi, T.F.M.P. Fülscher, L. Gagliardi, C. de Graaf, B.A. Hess, G. Karlström, R. Lindh, P.Å. Malmqvist, P. Neogrády, J. Olsen, B.O. Roos, B. Schimmelpfennig, M. Schültz, L. Seijo, L. Serrano-Andrés, P.E.M. Siegbahn, J. Stålring, T. Thorsteinsson, V. Veryazov, M. Wierzbowska, P.O. Widmark, MOLCAS Version 5.2, Lund University, Sweden, 2001.
[15] H.G. Yu, G. Nyman, J. Chem. Phys. 113 (2000) 8936.
[16] M.D. Feit, J.A. Fleck, A. Steiger, J. Comput. Phys. 47 (1982) 412.
[17] Á. Vibók, G.G. Balint-Kurti, J. Phys. Chem. 96 (1992) 8712.
[18] N. Marković, G.D. Billing, J. Chem. Phys. 100 (1994) 1085.
[19] P. Misra, C.W. Mathews, D.A. Ramsay, J. Mol. Spectrosc. 130 (1988) 419.
[20] S. Andersson, N. Marković, G. Nyman, Chem. Phys. 259 (2000) 99.